Energy Reports 9 (2023) 2169–2184

Contents lists available at ScienceDirect

Energy Reports

journal homepage: www.elsevier.com/locate/egyr

Research paper

Day-ahead optimal scheduling of smart electric storage heaters: A real quantification of uncertainty factors

A. Mugnini [a,*], F. Ferracuti [a], M. Lorenzetti [b], G. Comodi [a], A. Arteconi [a,c]

[a] Dipartimento di Ingegneria Industriale e Scienze Matematiche, Università Politecnica delle Marche, Via Brecce Bianche 12, 60131, Ancona, Italy
[b] Astea S.p.A., 60027 Ancona, Italy
[c] Department of Mechanical Engineering, KU Leuven, B-3000, Leuven, Belgium

ARTICLE INFO

Article history:
Received 14 September 2022
Received in revised form 21 December 2022
Accepted 3 January 2023
Available online 14 January 2023

Keywords:
Day-ahead optimal scheduling
Real-world implementation
Quantification of uncertainties
Smart electric storage heaters

ABSTRACT

Optimized controls are particularly promising for flexible and efficient management of space heating and cooling systems in buildings. However, when controls are based on predictive models, their effectiveness is affected by the reliability of the models used. In this paper we propose a quantification analysis of some of the main uncertainty factors that can be observed in an optimal control really implemented in a building. A day-ahead optimal scheduling was applied to the heating system (composed of smart electric heaters with thermal storage) of a single room in an office building located in Osimo (Italy). The control algorithm is formulated to determine the charging periods of the heaters with the objective of minimizing the withdrawal of energy from the grid. The control takes into account the electricity produced by a photovoltaic plant and must maintain the internal air temperature close to an imposed setpoint.

Firstly, the actual application of the control is shown during two selected days. Secondly, the analysis is extended to quantify the impact on the control performance of the prediction uncertainty of the input variables. The variable that has the greatest impact is the weather forecast and, specifically, the cloudiness index, which determines the solar gains. The different moment in time in which the weather forecast is predicted has proved to have a significant impact on the charging periods of the heaters (expected variation ranges from -50% to + 100%) and on the prediction of the indoor air temperature (variations observed up to 40%).

1. Introduction

In recent years, the application of advanced control techniques to manage thermal demand in buildings is attracting more and more interest (Dounis and Caraiscos, 2009). The building sector, indeed, has a high impact on the global energy demand. According to the International Energy Agency (IEA), the whole building sector is responsible for almost one-third of total global final energy consumption (International Energy Agency (IEA), 2022a), 22% of which due only to residential buildings (International Energy Agency (IEA), 2022c). Of the latter, the European Union has estimated that about 83.7% of the energy consumption is due to space heating (62.7%), space cooling (0.4%) and domestic hot water (15.1%) (Eurostat, 2022).

Another important factor is that the thermal demand of buildings has very favourable characteristics from the point of view of controllability. As known, the heat demand in buildings is needed to maintain an acceptable level of thermal comfort in the indoor environment (i.e., energy demand for space heating/cooling and domestic hot water) (Vakiloroaya et al., 2014). Given the possibility of decoupling demand from heat generation in buildings, this thermal demand has a great potential to be managed in a flexible way, while respecting the comfort constraints (Jensen et al., 2017). The decoupling capacity is made possible by different levels of thermal inertia in buildings. Examples are devices added to the emission system such as Thermal Energy Storage (TES) systems (Stinner et al., 2016) or the exploitation of the thermal mass of the building as a thermal storage (Ramos et al., 2019).

Another factor contributing to increasing interest in the advanced management of thermal demand in buildings can be identified in the increasing electrification of this energy demand. In recent years, indeed, the need to improve the penetration of Renewable Energy Sources (RESs) for decarbonization objectives, combined with the increasing availability of high-performance technologies (e.g., heat pumps with high efficiency), have led to a large diffusion of electrically powered heating and cooling systems in buildings (Hoseinpoori et al., 2022). In this regard, heat pumps are one of the most popular solutions. According to the IEA, the global stock of heat pumps increased nearly 10% per

* Corresponding author.
E-mail address: a.mugnini@univpm.it (A. Mugnini).

https://doi.org/10.1016/j.egyr.2023.01.013

year over the past 5 years, reaching the number of approximately 180 million heat pumps in use worldwide in 2020 (International Energy Agency (IEA), 2022b).

The electrification of the thermal demand of buildings gives to the control logic an even more important role. In fact, due to the non-programmability of the main RESs (such as photovoltaics or wind), the combination of thermal inertia with advanced control techniques can allow the optimal exploitation of energy sources while ensuring the comfort of the occupants. From a system perspective, this can lead to significant improvements in the security of the entire energy system by helping to balance the demand with the supply of energy.

Advanced control techniques differ from more traditional control techniques, such as Schedule-Based Controllers (SBCs) and Rule Based-Controllers (RBCs) (Krarti, 2018). SBC controls determine how the heating/cooling system of a building operates based on a pre-determined schedule (Barber and Krarti, 2022), while RBC are usually based on the monitoring of a specific parameter (e.g., power from RES or the room temperature) on which thresholds for the operation are set (i.e. the rule) (Péan et al., 2019). Although RBCs are more sophisticated than SBCs, they do not allow for a dynamic system management. Indeed, if real-time dynamic variations of boundary conditions are considered, more advanced control techniques need to be introduced. Advanced control techniques refer to smart controllers that can include optimal scheduling (Lu et al., 2015), optimal controls (Sampaio et al., 2021), artificial neural networks, adaptive fuzzy controls (Marvuglia et al., 2014) and machine learning or deep learning controls (Tien et al., 2022). Among these, one of the most popular is the Model Predictive Control (MPC) (Lyons et al., 2020) due to its capability of combining the principles of feedback control and numerical optimization (Serale et al., 2018).

In general, two key features can be distinguished in an optimal control based on the model of the system to be controlled: (i) the availability of prediction models and (ii) the solution of an optimization problem. The prediction models (i) shall be able to estimate the future behaviour of the system while its inputs can vary both in a controlled (manipulated variables) and in an uncontrolled (disturbances) way (Mugnini et al., 2020). These latter, when considering buildings, generally refer to the weather conditions and/or the behaviour of occupants (e.g., outdoor temperature, solar irradiance, and occupancy rate, etc Mugnini et al., 2021). Once the predictions of the future dynamics of the system are available, the optimal control solves an optimization problem (ii) to determine the control action: the optimizer minimizes an objective function respecting specific equality or inequality constraints (Mayne et al., 2000).

Optimal controls based on prediction models are so interesting for buildings because of the different advantages that can be obtained from their application. The main strengths are that, compared to other advanced controllers, they are relatively simple to formulate and do not have a fixed structure (i.e., modifications to the structure of the problem can be easily achieved). They also guarantee the achievement of an optimal solution and allow to easily consider hard constraints (Mugnini et al., 2022). On the other hand, these optimal controls have an important criticality that cannot always be overlooked: the strong dependence on the reliability of prediction models (Ceusters et al., 2021). In addition, real-world implementation can also be severely affected by incorrect or corrupted measured data (Drgoňa et al., 2020). The concomitant combination of these factors generates uncertainties on the reliability of the control. Indeed, according to Drgoňa et al. (2020), when referring to buildings, the most common uncertainties in MPCs arise from modelling errors (i.e., unknown parameters, inaccurate equations, or components not working according to specifications) and from the not reliable estimation of the uncontrolled inputs. This last case includes the prediction or the measurement of the outdoor temperature and the solar irradiation, as well as the inaccuracy of the sensors (e.g., inaccurate measurements or the availability of a limited number of sensors) or the presence of unmeasured disturbances (e.g., windows opening) (Drgoňa et al., 2020).

The quantification of the impact of these uncertainties on the effectiveness of an optimal control is a rather debated issue that question the large-scale spread of this type of control in buildings (Kontes et al., 2018). Several studies are available in literature that address model-related uncertainties in advanced controls. For instance, Hou et al. (2022) evaluated in a simulated environment the impact of the uncertainties related to the prediction of the weather data on the effectiveness of an MPC applied to a university building located in Norway. In this study the authors compared the performance of an RBC control with three types of MPC: an ideal one using perfect weather data and two configurations with different prediction models (a traditional numerical weather prediction model and one introduced by the authors). In particular, the authors highlighted a great dependence of the performance, in terms of savings and comfort, on the type of weather data used: weekly savings for heating costs of the ideal MPC compared with the RBC is 4.1%. This saving is reduced to zero (even with a worsening of comfort) in the case of MPC with the traditional numerical prediction model, while it becomes 3.4% with the model introduced by the authors. Also, Petersen and Bundgaard (2014) analysed the effect of the uncertainty of weather predictions on a predictive control in buildings. In their study the authors evaluated through energy simulations how buildings with different characteristics (e.g., orientation, thermal mass, solar shielding, and window area) are affected by changes in weather data predictions. An interesting result of this study is that buildings with high thermal mass seem to be less affected by errors in weather forecasting. On the other hand, lighter buildings were particularly sensitive to the accuracy of solar radiation forecasts.

These are just some examples extrapolated from the literature about the role of the uncertainties due to the prediction of the weather data on the performance of optimal control. Other works have assessed the effect of different sources of uncertainties. For instance, Sharma et al. (2022) evaluated the role of the estimation of occupancy profiles in a predictive control implemented in a commercial building. The authors concluded that with the introduction of an occupancy sensing system, the control could improve its performance by up to 5% (with also improvements in comfort) compared to a basic MPC that does not use specific occupancy information. An interesting aspect that also emerges from this study is that the performance of the control seems to depend significantly on the type of sensors used and on the non-idealities of sensors, such as bias and latency errors. Another important factor of uncertainty was assessed by Maasoumy et al. (2014), that evaluated the role of the model uncertainty in an MPC applied to buildings. In this case the uncertainty can derive both from the architecture of the model and from the numerical value of the parameters. Maasoumy et al. assessed a significant impact of parameters uncertainty on the effectiveness of the MPC and concluded that for models with high uncertainty (above 30%) it would be advisable to use a Robust Model Predictive Control (RMPC). On the basis of the conclusions of Maasoumy et al. (2014), in real-world applications of optimal controls based on prediction models, it would be better to use RMPCs or Stochastic Model Predictive Controls (SMPCs) (Oldewurtel et al., 2010). However, this significantly increases the complexity of the control, which in some cases may even not converge. For instance, the exact solutions for SMPCs for non-linear systems subject to non-gaussian disturbances are, in general, computationally not feasible (Hou et al., 2022; Ma et al., 2015).

It is therefore clear that the issue of the real-world application of optimal controls in buildings still attracts attention from the scientific community. One of the points on which many authors agree is that, when referring to the thermal demand of buildings, it is not yet clear to what extent the performance of the control (and therefore of the prediction model) are actually influenced by the uncertainty of individual contributions (i.e., the input variables and model architectures) (Lin et al., 2022).

The study presented in this paper fits into this context. Indeed, the intention is to propose a quantification of the impact of some factors of uncertainty on the effectiveness of an optimized control applied to a real building. In particular, the paper proposes the results obtained from the practical implementation of a day-ahead optimal scheduling to the electrical heating system of a single room in an office building. The heating system is composed of Smart Electric Heating Devices (SEHDs) equipped with a sensible TES. The objective of the control is to select the charging periods of the SEHDs to maintain the indoor air temperature in a comfort band and minimize the energy withdrawal from the grid. The controller also considers the availability of excess generation from a Photovoltaic (PV) plant installed in the building. The optimal control is based on data-driven models for the prediction of the system behaviour (building plus SEHDs) and of some inputs (e.g., solar gains and electricity availability from PV). By testing the control in a few days of operation, a quantification analysis of the impact of the uncertainties related to the predictions of the inputs is proposed. The input variables that affect control performance can be distinguished in direct (e.g., outdoor air temperature forecasting) and derived (e.g., solar and internal gains or excess of electricity from PV).

The objective of this study is to assess the weaknesses related to the implementation in the real world of a model-based optimal control. In fact, although the subject of uncertainty related to prediction models in advanced controls has already been discussed, there are not many examples of practical applications to quantify its impact. Therefore, this study wants to propose a practical case that can help to increase the knowledge on optimal controls applied to the management of space heating demand in buildings. Our goal is to provide an estimation of the individual effects of uncertainty factors, that can be useful for systems similar to the case study presented.

The rest of the paper is organized as follows. Section 2 contains the methodology with the mathematical formulation of the control. This section also describes the ways in which the inputs (both direct and derived) are obtained. Section 3 describes the main characteristics of the case study. In Section 4, on the other hand, the practical implementation of the control is presented while Section 5 reports the results of the validation of the models. Finally, Section 6 contains the main results of the application of the control together with the uncertainties quantification.

2. Methodology

This section describes the mathematical formulation of the optimal control. As mentioned, a controller based on a day-ahead optimal scheduling is formulized and practically implemented to a real case study. The case study is composed of a single room in an office building, whose demand for heating is met by two electric heaters with a thermal storage (i.e., SEHDs). The objective of the control is to select the best control actions (i.e., charge signal of the SEHDs) to minimize the withdrawal of electricity from the grid and keep the air temperature close to the setpoint. Being an optimal control, it requires a model that can predict the behaviour of the system together with the input variables. Based on the type of model required for their prediction, the input variables can be distinguished in (i) direct and (ii) derived. In the first two subsections the prediction models for the inputs are described (Section 2.1 for the direct and Section 2.2 for the derived input variables), while in Section 2.3 the mathematical formulation of the model of the system (building and SEHD) is provided. Finally, Section 2.4 contains the formulation of the optimization problem solved in the controller. To schematize the formulation of the control, Fig. 1 depicts the various parts of which the control is composed.

2.1. Direct input variables

Direct input variables are defined as those variables obtained without a physically based model, i.e. they refer to the predictions of weather conditions.

Thanks to an online weather service, the forecasts of the main weather data for the following 48 h (k) are available for each day. The quantities are: (i) the outdoor air temperatures ($T_{outdoorF_k}$ in °C), (ii) the incident solar irradiance (I_{F_k} in W m^{-2}), (iii) the wind speed (v_{F_k} in m s^{-1}) and (iv) the cloudiness index (Cl_{F_k} in %). Only the first three input variables are used for this optimal control, while the wind speed prediction is not used.

The weather forecasts are updated every hour, moving forward of 1 h the 48 h time of forecast. Therefore, the value of the input associated with k equal to 0 h in the subscript represents the present value of the input (actual weather conditions: $T_{outdoorF_0}$, I_{F_0}, v_{F_0} and Cl_{F_0}). It is worth pointing out that the weather data of the online service are not measured by a weather station but derived from numerical prediction models. Moreover, the trend of the variables appears strongly dependent on the time k when they are observed, making the performance of the control affected by the time of the forecast. k in fact represents the time when the control actions are calculated through the optimizer in the day ahead.

2.2. Derived input variables

Unlike direct input variables, derived inputs require a model for their estimation. These are essentially: (i) total heat gains (solar, internal gains) and (ii) the surplus of electricity generation from PV. The models for (i) and (ii) will be described in the next two subsections respectively.

2.2.1. Total heat gains

The model for the prediction of total heat gains is obtained with a data-driven model trained with historical data. Measurements are available every 15 min for the following quantities: (i) the indoor air temperature ($T_{a_{meas}}$ in °C), (ii) the illuminance (Lig_{meas} in lx) and (iii) the indoor relative humidity (in %), this latter is not used for the control.

Eq. (1) shows how total heat gains ($\dot{G}_{tot_k}$ in W) are calculated. In general, $\dot{G}_{tot_k}$ is assumed to be proportional to the expected illuminance index (Lig_{F_k} in lx) by a factor F_g. This choice is supported by the fact that, from the observation of historical data, the measured indoor air temperature ($T_{a_{meas}}$) shows a rather high correlation with the Lig_{meas}, on average around 65% and 75% on clear days. Lig_{F_k} is in turn obtained as the sum of two components: the incident solar radiation ($\dot{S}_{sol_F}$ in W) and the internal gains ($\dot{S}_{int_F}$ in W). To assess the solar radiation entering the room, the prediction of the cloudiness (Cl_{F_k}) was also considered. For this reason, $\dot{G}_{tot_k}$ also depends on the time k in which the prediction of direct inputs is observed (see Section 2.1).

$$\dot{G}_{tot_k} = F_g Lig_{F_k} = F_g \left[\frac{\dot{S}_{sol_F}(1 - Cl_{F_k}/100)}{100} + \dot{S}_{int_F} \right] \quad (1)$$

The incident solar radiation ($\dot{S}_{sol_F}$) is obtained according to the approach reported in the Italian standard UNI/TS 11300-1:2014 (UNI

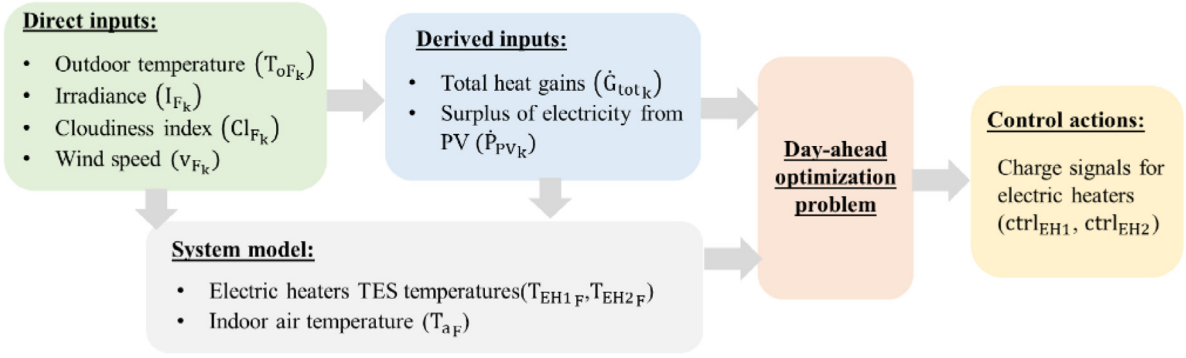

Fig. 1. Schematic of the flow chart of the day-ahead optimal scheduling control.

(Italian Standard Organization), 2014), with which, starting from the location, the inclination of the surface and the characteristics of the windows, the solar inputs through the transparent components can be calculated. The internal gains due to artificial lighting ($\dot{S}_{int_F}$), instead, are modelled according to a parabolic profile (Eq. (2)).

$$\dot{S}_{int_F}(h) = ah^2 + bh + c \quad \text{for } h = 1, \ldots, 24 \tag{2}$$

where h indicates the hour of the day and the coefficients a, b and c, are obtained with a training process.

2.2.2. Surplus of PV generation

Using the historical data of the electrical consumption of the building and of the PV production, it has been estimated the probability that in a specific hour of the day (h) there can be an excess of PV generation above a minimum threshold ($\dot{P}_T$ in W). A probability density function (pdf) for the PV surplus was therefore defined. To also consider the effect of the daily cloudiness, the multiplicative factor F_{PV_k}, which is based on the predicted cloudiness index (Cl_{F_k}), is also introduced:

$$\text{for } h = 1, \ldots, 24$$

$$F_{PVk}(h) = \begin{cases} \dfrac{(100 - Cl_{F_k}(h)/100)}{100} & \text{if } I_{F_k}(h) > 0 \\ 0 & \text{if } I_{F_k}(h) \le 0 \end{cases} \tag{3}$$

Consequently, the availability of excess of PV generation ($\dot{P}_{PV_k}$ in W) is estimated by:

$$\text{for } h = 1, \ldots, 24 \quad \dot{P}_{PV_k}(h) = p_{PV} \cdot F_{PV_k}(h) \cdot pdf(h) \cdot I_{F_k}(h) \tag{4}$$

where the parameter p_{PV} has been added to calibrate the model with the measured data, whose numerical value is obtained with training.

Based on Eqs. (3) and (4), it emerges the dependence of the PV surplus prediction on the direct input irradiance I_{F_k} and cloudiness Cl_{F_k}. For this reason, similarly to what discussed about the total heat gains forecasting (Section 2.2.1), the uncertainty in the prediction of PV surplus generation is strongly correlated with the reliability of the direct inputs and with the time in which they are evaluated (k).

2.3. System prediction model

The description of the dynamics of the system is entrusted to the prediction of the state of charge of the SEHDs and of the internal air temperature (T_a). For this reason, it has been developed a model to represent both the dynamics of the SEHDs and the thermophysics of the room, i.e., T_a. In the next two subsections the model is described by dividing the equations for the SEHDs (Section 2.3.1) by those for the indoor air temperature (Section 2.3.2). They constitute the model used in the optimal control.

2.3.1. Smart Electric Heating Device model

Each SEHD is modelled as a single heat node associated with a capacitance C_{EH} (in Wh K^{-1}) and a temperature T_{EH_F} (in °C). These refer to the bricks contained within the Electric Heater (EH) that act as TES. The thermal power with which the TES is charged is expressed by the product between a charge signal ($ctrl_{EH}$, 1/0 signal) and the charging power ($\dot{Q}_{EH}$ in W). On the other hand, the discharge power of the SEHD is represented by the polynomial expression reported in the square brackets in Eq. (5), including both environmental losses and the heating fan action (coefficients l_0, l_1, l_2 whose numerical value are obtained with the training process).

$$C_{EH}\frac{dT_{EH_F}}{dt} = \dot{Q}_{EH}ctrl_{EH} - \left[l_0 + l_1\left(T_{EH_F}\right) + l_2\left(T_{EH_F}\right)^2\right] \tag{5}$$

2.3.2. Room model

The model of the controlled room consists of a lumped concentrated parameters model based on a network of resistances and capacities (RC-networks). RC networks are in fact one of the most common modelling architectures in the field of modelling the energy demand of buildings (Li et al., 2021). The specific architecture of the network was built by the authors, inspired by the model proposed by Boodi et al. (2020) who suggest modelling the building envelope components facing outwards as RC networks with 2 capacities and 3 thermal resistances. The room model is composed of 3 thermal nodes (Fig. 2). The first (T_{aF}, C_a) represents the temperature of the internal air (variable to be provided to the thermostat), while the nodes (T_{waF}, C_{wa}) and (T_{woF}, C_{wo}) represent respectively the mass of the building envelope towards the internal air (from the thermal insulation to the inside) and towards the external temperature ($T_{outdoorF_k}$). The heat power flux between nodes is regulated by thermal conductance: K_{wa}, K_{wind}, K_{wins}, K_{wo} (in W K^{-1}). The total heat gains are expressed by $\dot{G}_{tot_k}$ (Eq. (1)). The heat losses of each SEHD are modelled with a conductance ($K_{l_{EH}}$), while the heating power provided by the activation of the fan is modelled as a heat flux proportional (f_{FAN}) to the temperature of the storage in the SEHD and is regulated by the control signal $ctrl_{FAN}$ (1/0 signal). In summary, Eqs. (6)–(8) represent the model of the controlled room.

$$\begin{aligned} C_a\frac{dT_{a_F}}{dt} = {} & \dot{G}_{tot_k} + K_{wa}\left(T_{wa_F} - T_{a_F}\right) + K_{wind}\left(T_{outdoorF_k} - T_{a_F}\right) \\ & + K_{l_{EH1}}\left(T_{EH1_F} - T_{a_F}\right) \\ & + K_{l_{EH2}}\left(T_{EH2_F} - T_{a_F}\right) + ctrl_{FAN1}f_{FAN1}\left(T_{EH1_F}\right) \\ & + ctrl_{FAN2}f_{FAN2}\left(T_{EH2_F}\right) \end{aligned} \tag{6}$$

$$C_{wa}\frac{dT_{wa_F}}{dt} = K_{wa}\left(T_{a_F} - T_{wa_F}\right) + K_{wins}\left(T_{wa_F} - T_{wa_F}\right) \tag{7}$$

$$C_{wo}\frac{dT_{wo_F}}{dt} = K_{wo}\left(T_{oF_k} - T_{wa_F}\right) + K_{wins}\left(T_{wa_F} - T_{wa_F}\right) \tag{8}$$

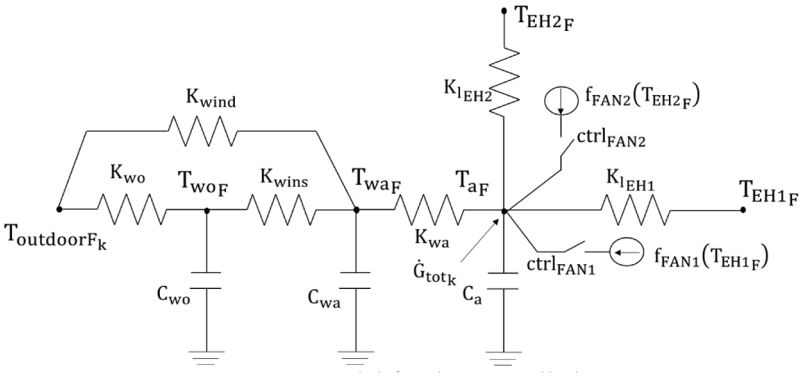

Fig. 2. RC model for the controlled room.

2.4. Optimization problem

As mentioned, the controller is based on the day-ahead solution of an optimization problem. The objective is to minimize the electricity withdrawal from the grid and maintain the indoor air temperature close to the imposed setpoint ($T_{a_{th}}$):

$$\text{minimize}\left(\sum_{t=1}^{24}\left[w_1(t)\,\dot{Q}_{EH1}(t)\,ctrl_{EH1}(t) + w_1(t)\,\dot{Q}_{EH2}(t)\,ctrl_{EH2}(t) + w_2\left|T_{a_{th}}(t) - T_{a_F}(t)\right|\right]\right) \quad (9)$$

where: w_1 and w_2 are the weights assigned to the individual objectives (i.e., electricity withdrawal and maintaining the air temperature setpoint). The decision variables of the optimization problem are the charging and the discharging signals for the SEHDs ($ctrl_{EH1}(t)$, $ctrl_{EH2}(t)$, $ctrl_{FAN1}(t)$ and $ctrl_{FAN2}(t)$).

The availability of the electrical power from PV is included in the optimization problem through the weight factor w_1. The trend of w_1 has been calibrated to incentivize the charge in periods where excess of generation from PV is predicted by the model (Eq. (4)). In particular, the weight w_1 assumes the values given in Eq. (10).

$$\text{for } t = 1,\ldots,24 \quad w_1(t) = \begin{cases} 0.5 & \text{if} \quad \dot{P}_{PV_k}(t) > \dot{P}_T \text{ kW} \\ 10 & \text{if} \quad \dot{P}_{PV_k}(t) \le \dot{P}_T \text{ kW} \end{cases} \quad (10)$$

To the weight w_2 was assigned a numerical value of 0.5. The values have been identified in an empirical way. However, it should be noted that the operation of the control could be strengthened in one direction (to maximize the self-consumption of PV) or in the other (to maintain the setpoint) by varying the numerical value of the weights w_1 and w_2.

The constraints applied to the problem are expressed by the following equations:

$$\text{for } t = 1\ldots24 \quad T_{a_{th}}(t) - \Delta T_{sp} \le T_{a_F}(t) \le T_{a_{th}}(t) + \Delta T_{sp} \quad (11)$$

$$\text{for } t = 1\ldots24 \quad T_{EH\,min} \le T_{EH1_F}(t) \le T_{EH\,max} \quad (12)$$

$$\text{for } t = 1\ldots24 \quad T_{EH\,min} \le T_{EH2_F}(t) \le T_{EH_{max}} \quad (13)$$

where ΔT_{sp}(in °C) is the thermostat deadband and $T_{EH_{min}}$ and $T_{EH_{max}}$ are respectively the minimum and the maximum temperatures that the storage materials in the SEHD can reach.

The objective function and the constraints of the optimization problem are related to the decision variables by the model of the system to be controlled which, as described in the previous subsections, is represented by Eqs. (5)–(8).

As expressed in Eqs. (9)–(13), the problem has a nonlinear formulation. It is solved in Python as Mixed integer nonlinear programming (MINLP) with the GEKKO Optimization Suite (Beal et al., 2018).

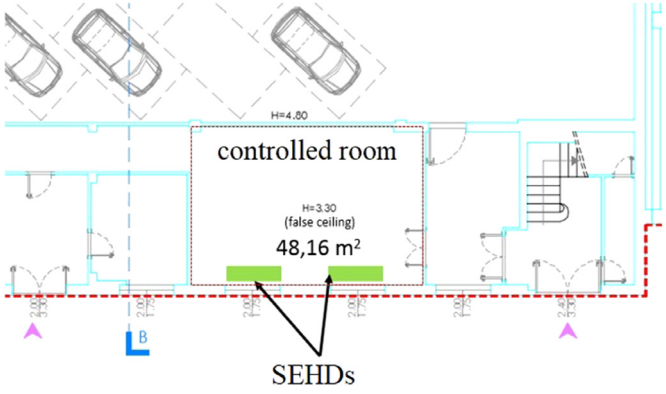

Fig. 3. Controlled room with SEHDs.

3. Case study

The day-ahead optimal scheduling is applied to a single room within the ASTEA headquarters, an office building located in Osimo (43°29′09.89″N 13°28′55.56″E), Central Italy. The floor plan of the room is shown in Fig. 3.

The room is on the ground floor. It has a floor area of 48.16 m^2 with a single vertical wall facing outwards (south-east exposure) in which are located two windows that occupy about 7 m^2. The other perimeter walls are arranged either towards heated rooms (south-west and north-east exposure) or towards unheated rooms (north-west exposure). The external wall is a cassette masonry wall, with 4 cm of thermal insulation (i.e., rock-wool panel). The value of the thermal transmittance is 0.48 W m^{-2} K^{-1} for the external wall in accordance with UNI TS11300-1 (UNI (Italian Standard Organization), 2014), UNI EN ISO 6946 (UNI (Italian Standard Organization), 2018a) and UNI EN ISO 13370 (UNI (Italian Standard Organization), 2018b). The windows have a thermal transmittance equal to 1.81 W m^{-2} K^{-1} in accordance with UNI EN 12831 (UNI (Italian Standard Organization), 2018c), UNI EN ISO 6946 (UNI (Italian Standard Organization), 2018a) and UNI EN ISO 10077 (UNI (Italian Standard Organization), 2018d). The building is also equipped with PV plants with a nominal electric power of 78.14 kW_p installed on site.

As for SEHDs, two devices from the company Glen Dimplex Heaters (GDHs) are installed in the room (Glen dimplex, 2022). A GDH is an electric space heater equipped with a thermal storage, composed of bricks. As detailed in the next section, this device allows to apply advanced control on the charging of the storage material. The technical specifications of the two GDHs installed in the room are showed in Table 1.

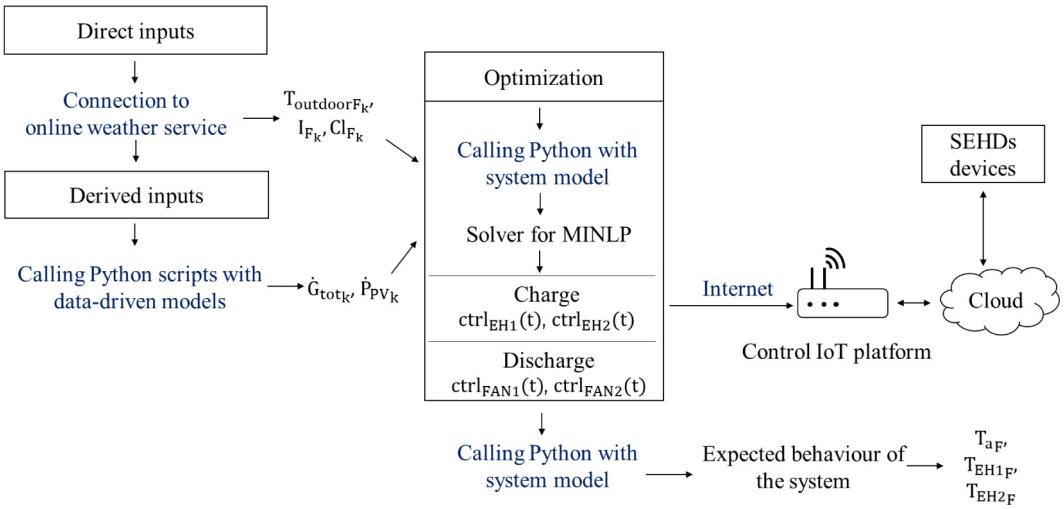

Fig. 4. Schematic of the day-ahead optimal scheduling implementation and communication mode.

Table 1
QM100 SEHD technical specifications (UNI (Italian Standard Organization), 2018c).

Input rating +5%/−10% (W)	Output rating (W)	Boost mode rating (W)	Maximum storage capacity (Wh)
2220	1000	800	15 540

The two devices are monitored in real time. In particular it is possible to monitor the trends (with a timestep of 15 min) of: (i) the indoor air temperature ($T_{air_{meas}}$), (ii) the illuminance (Lig_{meas}), (iii) the charge signals of the SEHDs ($ctrl_{EH1_{meas}}$ and $ctrl_{EH2_{meas}}$), (iv) the discharge signals of the SEHDs ($ctrl_{FAN1_{meas}}$ and $ctrl_{FAN2_{meas}}$), (v) the temperature of the core of each SEHDs ($T_{EH1_{meas}}$ and $T_{EH2_{meas}}$) and (vi) the electrical power exchanged at the general meter ($\dot{P}_{e_{meas}}$ in kW_e). The latter variable (vi) can assume both positive and negative values (for withdrawals or inputs into the grid). Taking only the negative values associated with $\dot{P}_{e_{meas}}$, the vector of generation excesses from PV can be obtained ($\dot{P}_{PV_{meas}}$ in W).

4. Practical implementation of the optimal scheduling control

Fig. 4 represents a schematic of the implementation of the day-ahead optimal scheduling. As described in the previous sections, each day, both direct and derived inputs must be predicted according to the methodology discussed in Section 2. Then, the optimization problem for the next day is solved. In this way the values of the charge and discharge signals for the SEHDs are obtained ($ctrl_{EH1}$, $ctrl_{EH2}$, $ctrl_{FAN1}$ and $ctrl_{FAN2}$).

Each SEHDs can communicate with a Control IoT (Internet of Things) platform, developed and made available by the manufacturer, that allows the connection with the cloud, which enables the transmission, storage, and retrieval of telemetry information. The control developed in Python can communicate the schedule for the device and by-pass the on-board controller. Every day, therefore, the control signals obtained from the optimization are sent to each SEHD that are forced to charge in the indicated time bands. On the other hand, it is not possible to have a direct control on the discharge, that is regulated by the thermostat setpoint.

5. Validation of the model

This section shows the results of the training and the testing of the various components of the model implemented in the control. In the first two Sections (5.1 and 5.2), the models for the prediction of derived input variables are addressed while in Section 5.3 models of SEHD and controlled room are discussed.

Table 2
Result of the training and test process for Light prediction.

Period	RMSE (lx)	Error (%)
2–20 March 2022 (training)	117.8	3.7
24–31 March 2022 (test)	82	5.7
15–22 April 2022 (test)	105	9.0

5.1. Total heat gains

Since, as already described in Section 2.2.1, the correlation between daily trends in indoor air temperature and illuminance index is on average between 65% and 75% on clear days, the total heat gains input is assessed in relation to the variable Lig_{meas} (i.e., measured values). The comparison between the measured illuminance index and the one predicted by the model is shown in Fig. 5. Fig. 5 refers to the training period: from the 2nd to the 20th of March 2022. A Root Mean Square Error (RMSE) of 117.8 lx is obtained, that compared with the maximum variation of the measured magnitude (about 3000 lx) represents an error of 3.7%. Table 2 compares the performance of the model in terms of RMSE and percentage error between the training period and two different test periods. By observing the values shown in Table 2, it is possible to conclude that the prediction capacity of the model for the Lig quantity is good as the error remains below 10% both in training and in test.

5.2. Surplus of PV generation

A Gaussian probability distribution was chosen for the probability density function (pdf) in Eq. (4). The mean value (11.8 h) and the standard deviation (1.8 h) of pdf were obtained from the observation of the measured data. For each hour in each day, it has been assessed the number of occurrences in which the surplus generation from PV exceeded the threshold ($\dot{P}_T$ set to 4 kW_e) for each hour in each day. Fig. 6 represents the results of the training process for the PV model. The RMSE in training (2–20 March 2022) is 1.72 kW_e, with a percentage error of 4.2%,

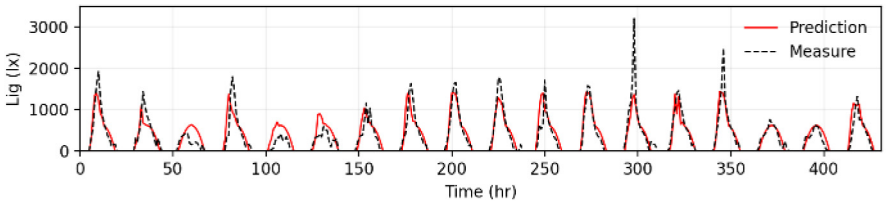

Fig. 5. Comparison between measurements and model prediction for illuminance (training, 2–20 March 2022).

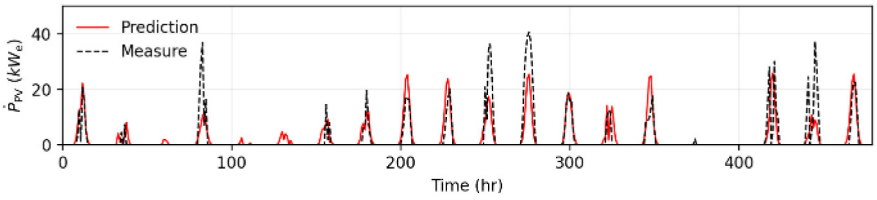

Fig. 6. Comparison between measurements and model prediction for PV surplus production (training, 2–20 March 2022).

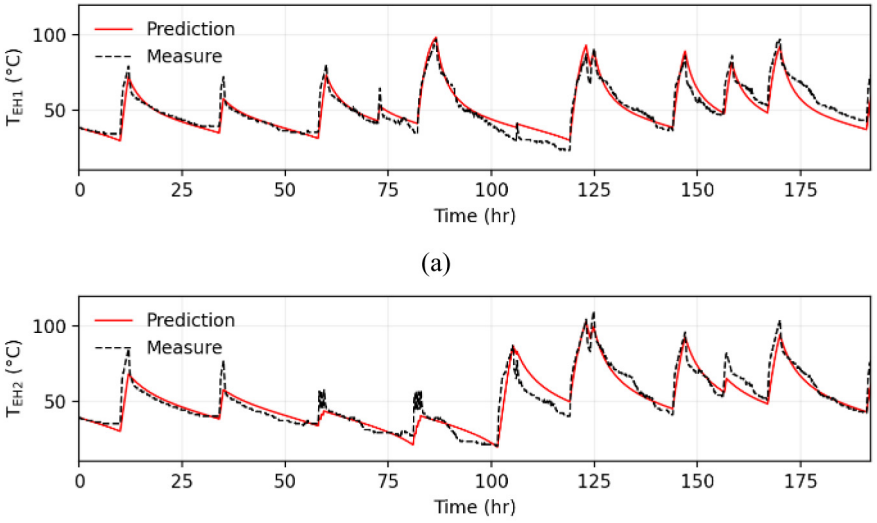

Fig. 7. Comparison between measurements and model prediction for SEHDs temperatures (training, 24–31 March 2022): (a) Heater 1 and (b) Heater 2.

Table 3
Result of the training and test for PV excess availability model.

Period	RMSE (kW_e)	Error (%)
2–20 March 2022 (training)	1.76	4.3
24–31 March 2022 (test)	2.1	5.7
15–22 April 2022 (test)	3.5	7.0

Table 4
Result of the training and test for the model of SEHDs.

Period	RMSE (°C)		Error (%)	
	Heater 1	Heater 2	Heater 1	Heater 2
24–31 March 2022 (training)	4.1	4.4	5.5	4.9
12–19 March 2022 (test)	5.7	7.2	8.3	9.9
2–7 April 2022 (test)	8.3	6.6	13.1	9.1

that is similar to the error obtained in the test. Table 3 reports the RMSE and the relative error in training and in two test periods. Also in this case, errors of less than 10% are obtained both in the validation and in the test, confirming a good prediction performance of the model.

5.3. System model: SEHDs and room

Fig. 7 represents the comparison between the temperature of the storage material in the SEHD measured and predicted by the model. The training is for one week, from 24 to 31 March 2022. During training, the model has a RMSE of 4.1 °C for Heater 1 and a RMSE of 4.4 °C for Heater 2. The measurement errors, assessed against the maximum measurement variations, are respectively 5.5% and 4.9%.

Considering the model of the controlled room, the training results are shown in Fig. 8 and Table 5 respectively. In this case the model has been trained with the measured input variables (Lig_{meas} is used for the total heat gains radiation and $T_{outdoorF_0}$ for the outdoor air temperature).

The model has an RMSE of 0.65 °C during training with a relative error related to the maximum variance of the measured air temperature of about 9.5% (Table 5). If the model for predicting the thermal dynamics of the temperatures of the storage materials has shown good performance (error less than 10% both in testing and in training, Table 4), significantly worse performance

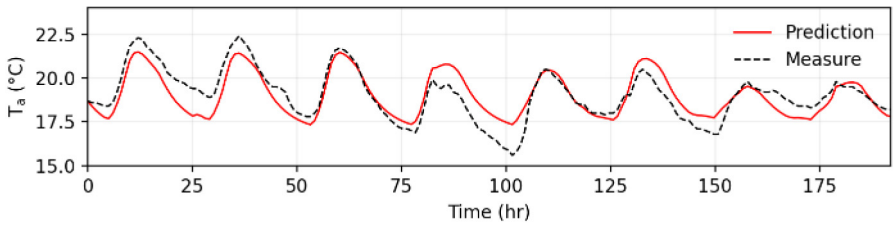

Fig. 8. Comparison between measurements and model prediction for the air temperature of the controlled room model (training, 24–31 March 2022).

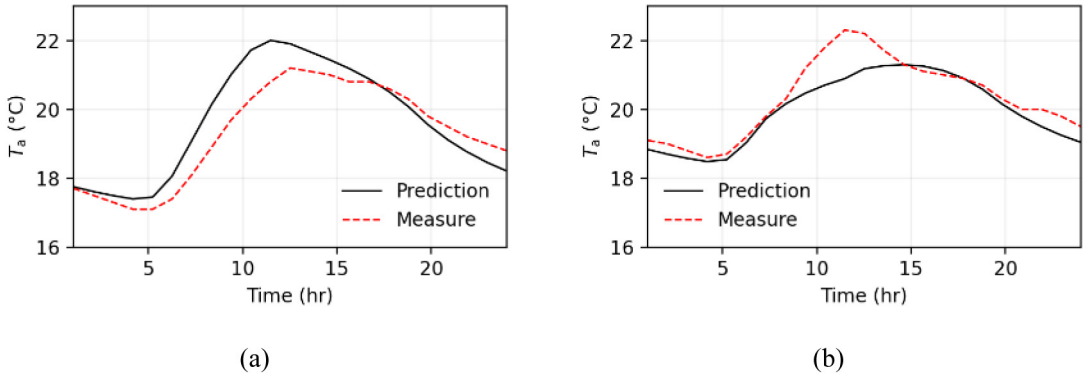

Fig. 9. Comparison between measurements and model prediction for air temperature (T_a): (a) 2nd of May 2022 and (b) 4th of May 2022.

Table 5
Result of the training and test for air temperature: controlled room model.

Period	RMSE (°C)	Error (%)
24–31 March 2022 (training)	0.65	9.5
12–19 March 2022 (test)	0.84	15.9
2–7 April 2022 (test)	0.94	16.2

Table 6
Indoor air temperature model: results of test in single days (12–19 March 2022).

Day	RMSE (°C)
12/03/2022	0.41
13/03/2022	0.35
14/03/2022	2.23
15/03/2022	0.55
16/03/2022	1.26
17/03/2022	0.33
18/03/2022	0.48
19/03/2022	0.43

was assessed during the test periods in the indoor air temperature prediction model. This behaviour is due to the presence of abnormal days in which the measured air temperature shows a trend not easily predictable in relation to the trend of the inputs. This fact does not exclude the occurrence of random events, such as the opening of a window that can affect the goodness of the model. For example, by testing the model on individual days in 12–19 March 2022, the value of the RMSE value has been evaluated for each day (Table 6). It is clear the presence of two abnormal days (14/03 and 16/03) in which the RMSE exceeds 1 °C.

6. Results

This section presents the results of the implementation of the day-ahead optimal scheduling control together with an analysis of the factors that determine the uncertainties of its application. In particular, the section is divided into two subsections: Section 6.1 in which two days when the control has been applied to the building are described and Section 6.2 where a sensitivity analysis to quantify the impact of uncertainty factors is presented.

6.1. Real implementation of the control

The control has been effectively applied to the room in two days: the 2nd and the 4th of May 2022. In Fig. 9, a comparison can be made between the temperature of the internal air predicted by the model in the control and the actual measured. The model has proven effective in predicting air temperature, in fact an RMSE of 0.52 °C is obtained for the 2nd of May, while 0.36 °C for the 4th. In these two days the weather forecasts were observed in two different hours: at 3.00 pm (k equal to 15) for May 2nd and at 6.00 pm (k equal to 18) for May 4th.

Figs. 10 and 11 show, instead, the comparison between expected and measured input variables: Light (Lig) and surplus of electricity from PV, respectively. On the 4th of May (Fig. 10b), the Lig quantity predicted has an RMSE of 75 lx (with a maximum difference between prediction and measurement of 269 lx), while the value become 148 lx (maximum difference of 624 lx between prediction and measurement) on the 2nd of May (Fig. 10a). The prediction of PV surplus generation is shown in Fig. 11 according to a 1/0 signal representing availability (1) or non-availability (0) of electrical power form PV greater than 4 kW_e. This choice was made to show a quantity in line with the weight factor used in the optimization problem (Eq. (10)). It should be noted that, while on May 2nd the expected (prediction in Fig. 11) availability interval is the line with the measured one, although more conservative, on May 4th the prediction was not accurate. This is due to the fact that the prediction of the derived inputs is strongly linked to the forecast of the direct input variables (in particular the cloudiness index). If these do not reflect what is happening in the reality, the prediction is not reliable. This in general is an issue that cannot be neglected when reliable measurements of the external conditions (e.g., access to nearby weather stations) are not available. Indeed, in the days shown in Fig. 12, the direct inputs greatly influence the derived inputs predictions. Their influence on the control will be described in the next Section 6.2.

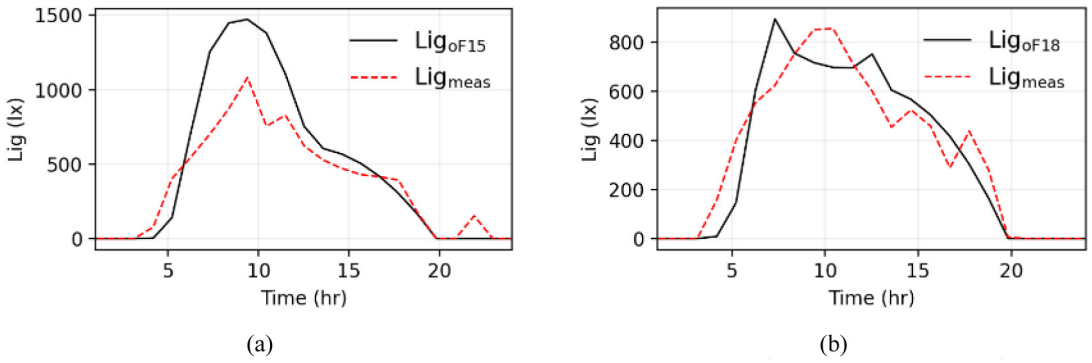

Fig. 10. Comparison between measurements and model prediction for Lig: (a) 2nd of May 2022 and (b) 4th of May 2022.

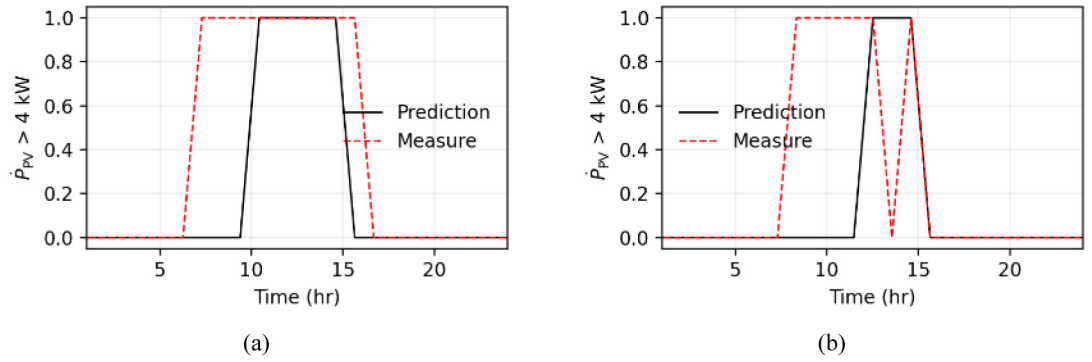

Fig. 11. Comparison between measurements and model prediction for PV surplus production (1 signal if there is excess electricity greater than 4 kW, 0 otherwise): (a) 2nd of May 2022 and (b) 4th of May 2022.

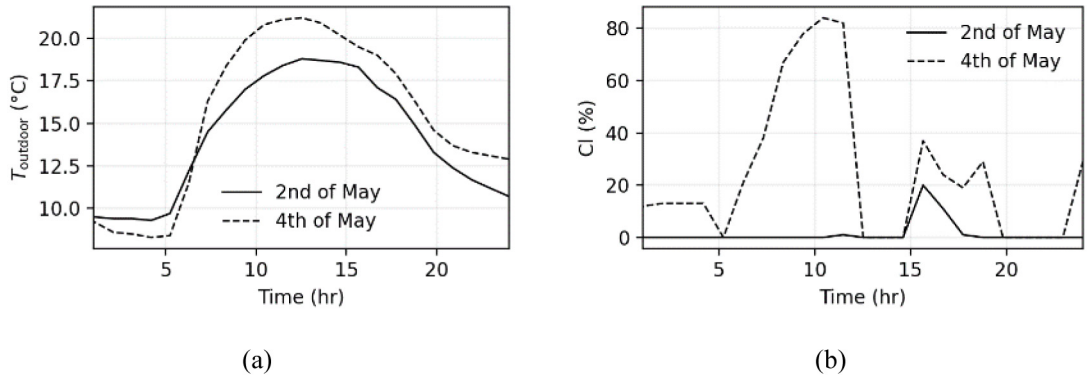

Fig. 12. Weather forecast obtained the day before: (a) Outdoor air temperature ($T_{outdoor}$) and (b) Cloudiness index (Cl).

Figs. 13 and 14 show the comparison (measured/prediction) between the temperatures of the storage material in electric heaters (i.e., the temperature of the cores). Considering the results on the 2nd of May (Fig. 13), an RMSE of 1.44 °C is observed, which corresponds to an error of 4.7% with respect to the maximum variation of the measured temperature in the first SEHD (Fig. 13a). For the second SEHD (Fig. 13b) the RMSE become 2.03 °C with an error of 8.4%. The correspondence between prediction and measured temperature of the SEHDs storage worsens on May 4th (Fig. 14). On this day the RMSE becomes 3.8 °C for the first heater (Fig. 14a), with an error of 11.4%, while it is 3.54 °C for the second device (Fig. 14b), which corresponds to an error of 13.2%. This depends on the fact that at the end of May 4th there were probably some connection malfunctions between the remote control and the devices. In fact, observing Fig. 14 it can be seen that after 8.00 pm the temperatures of the storage materials started to rise, even if a charge signal other than 0 was never sent by the control logic.

To conclude, the charge signals obtained from the optimal control, that have been sent to the devices, activate the charge in the time slots between 10.00 am and 11.00 am on the 2nd of May and between 12.00 pm and 1.00 pm on the 4th of May. Looking at Fig. 11 it can therefore be inferred that in the case of the 2nd of May (Fig. 11a), the control was effective in charging at the same time as surplus PV generation was available, whereas in the 4th of May the control was not at all effective in predicting the availability of the free source (Fig. 11b). In the first case, therefore, the withdrawal of electricity from the grid is zero while in the second case there is a withdrawal of about 4.4 kWh$_e$.

6.2. Quantification of uncertainty factors

To deepen the analysis of the role of uncertainty factors, the first day was selected (the 2nd of May 2022). This section is

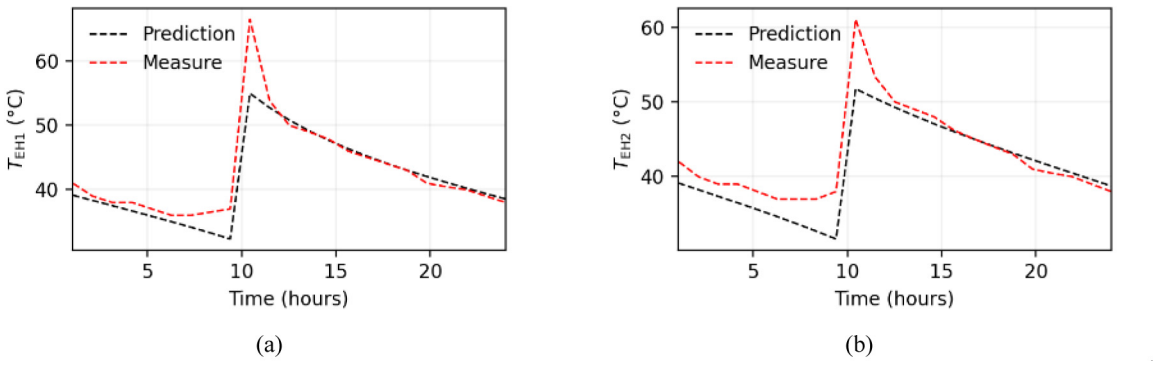

Fig. 13. Comparison between measurements and model prediction for SEHDs (temperature of the storage material) on 2nd of May 2022: (a) Heater 1 and (b) Heater 2.

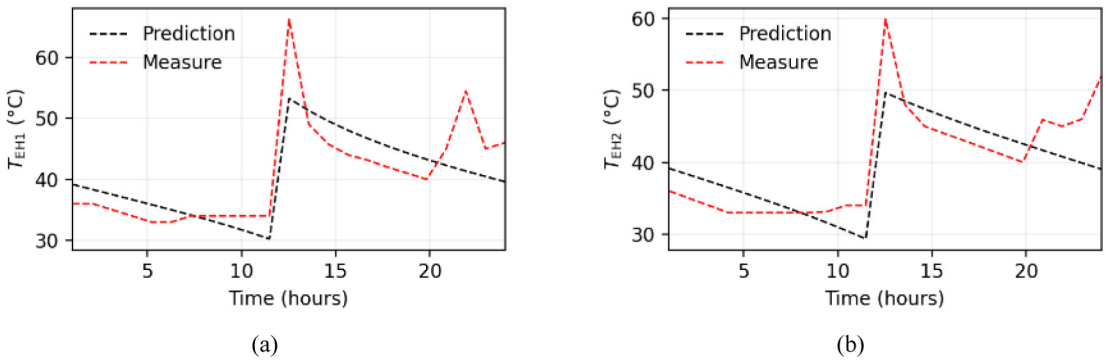

Fig. 14. Comparison between measurements and model prediction for SEHDs (temperature of the storage material) on 4th of May 2022: (a) Heater 1 and (b) Heater 2.

divided into two subsections, in the first one (Section 6.2.1), the impact of the direct input forecast on derived inputs estimation is analysed, while in the second (Section 6.2.2) a quantification of how the uncertainty factors affect the performance and the effectiveness of the control is presented.

6.2.1. Uncertainty factors on the derived input

Starting the analysis from direct input variables, Fig. 15 shows how the trend of the outdoor air temperature and the index of cloudiness vary depending on the time k at which the forecast is made. This behaviour has not been analysed for the irradiance as it does not show any change with the forecast time (estimated as a function of the geographical location only). Observing the hourly standard deviation of the input variables (Fig. 16), the variability of the forecast appears rather contained for the outdoor air temperature (the standard deviation remains below 0.6 °C, Fig. 16a). On the other hand, the cloudiness index (Fig. 16b) is much more variable with k (standard deviation is above 20% most of the time). As can be expected, this variability has a strong impact on both the derived inputs and, consequently, on the prediction capability of the controlled room model.

Analysing the derived inputs, the total heat gains are strongly linked to the measurable quantity Lig. Referring to the model expressed by Eq. (1), it can be noted that the prediction of the total heat gains is affected by the time k at which the direct inputs are observed the day before, as the cloudiness index intervenes (Cl_{F_k}) in the formulation. Fig. 17 shows the link between the variation of Lig_{F_k} (illuminance forecasted at time k) respect to the measured value (Lig_{meas}) and the average cloudiness index in the hours when incident solar radiation is expected by varying k (time of observation). In Fig. 17 both the percentage variation of the daily integral of Lig_{F_k} compared to the measured one (black curve) together with the estimated percentage error (red curve) are reported. The integral variation has been calculated to quantify the error on the estimation of total heat gains.

What can be noted by looking at Fig. 17 is that the deviation between the measured and the predicted values tends to increase as the average cloudiness index decreases. The lowest percentage error (about 8.2%) is obtained with the maximum average cloudiness index (about 39.3%). Looking further at the percentage variation in the integral of Lig, it is observed that for all the hours of prediction k, Lig_{F_k} is overestimated with respect to Lig_{meas}. This is probably due to the fact that for every time k, Cl_{F_k} may actually be underestimated compared to what is currently happening. In fact, if Eq. (1) is reversed to derive the trend of the Cl that would allow to predict the measured value of Lig_{meas}, the dashed curve in black in Fig. 18 is obtained. Comparing this with the trends of the Cl_{F_k}, a general underestimation of Cl can be confirmed.

As for the prediction of surplus PV generation ($\dot{P}_{PV_k}$), according to Eq. (3), this depends both on the prediction of Irradiance (I_{F_k}) and once again on C_{F_k}. As already mentioned, I_{F_k} that is extrapolated from the weather service does not seem to depend on the hour k, also in this case, the impact of the variability of the C_{F_k} on the $\dot{P}_{PV_k}$ prediction is evaluated. For the purpose of solving the optimization problem in the control, the percentage of time in which an excess of more than 4 kW_e is expected (estimated power to load the SEHD) is taken into account. Fig. 19 shows the percentage of daily hours in which the predicted excess of more than 4 kW coincides with the measured (black line) and the average Cl in the hours of measured PV surplus as function of the time k. When compared with the average C_{F_k}(red line), a clear dependency such as that observed in Fig. 17 is less evident. However, the percentage of time in which the PV prediction is simultaneous with the measured values varies between 21% and 47% by varying the cloudiness index. Measured and predicted PV surplus tend to be closer when the average cloudiness factor

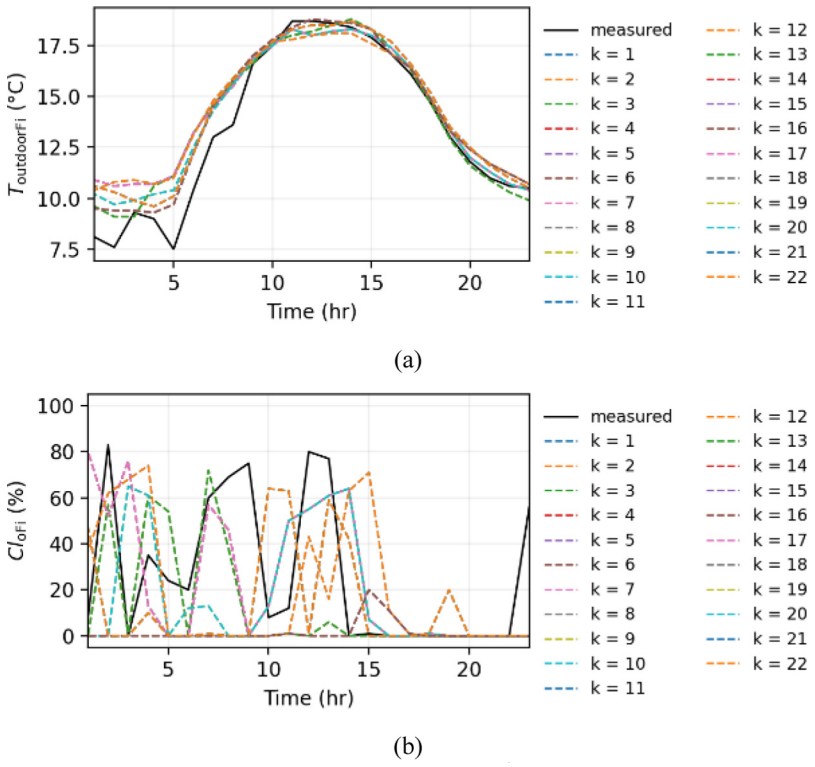

Fig. 15. Direct input variables depending on the time of the forecast (2nd of May 2022): (a) outdoor air temperature ($T_{outdoor}$) and (b) cloudiness index (Cl).

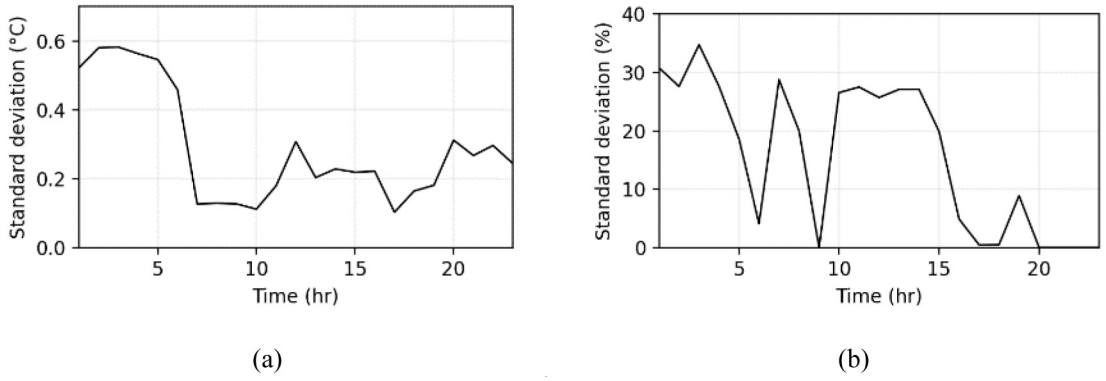

Fig. 16. Direct input variables hourly standard deviation (2nd of May 2022): (a) outdoor air temperature ($T_{outdoor}$) and (b) cloudiness index (Cl).

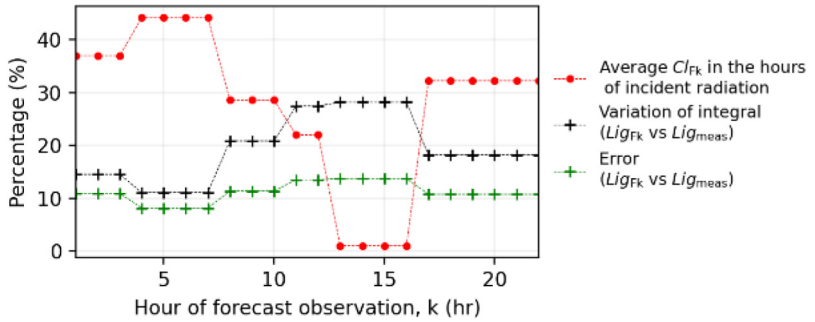

Fig. 17. Percentage variation of the daily integral of Lig (prediction vs. measured), relative error for Lig (prediction vs. measured) and average Cl in the hours of incident solar radiation as function of the time k in which the direct inputs are observed the day before (2nd of May 2022).

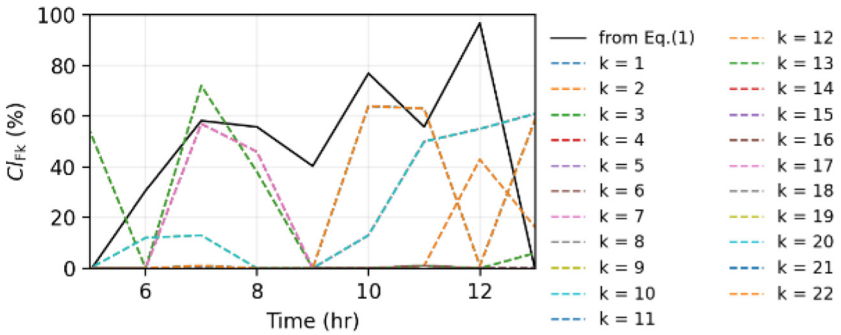

Fig. 18. Cl in the hours of incident solar radiation as function of the time k in which the direct inputs are observed the day before compared to Cl obtained by Eq. (1) with the illuminance equal to Lig_{meas} (2nd of May 2022).

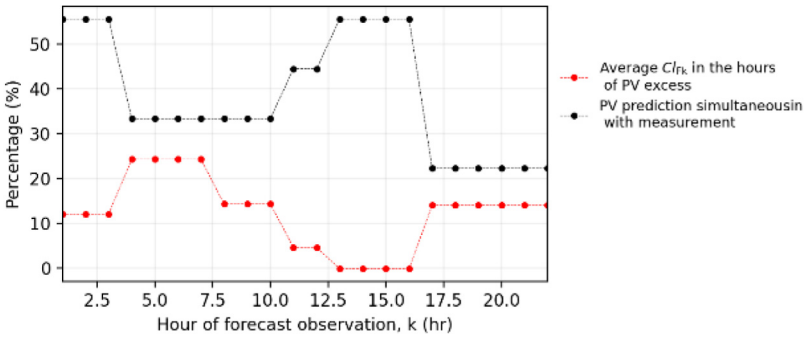

Fig. 19. Percentage of daily hours in which the predicted PV surplus of more than 4 kW coincides with the measured and average Cl in the hours of measured PV excess as function of the time k in which the direct inputs are observed the day before (2nd of May 2022).

decreases, however this is not observed on a regular basis (for example, for k greater than 16 there is a lower average Cl than between 4 and 7, however the percentage of coincidence between PV prediction and measure is lower in the first case than in the second).

6.2.2. Uncertainty factors on the performance of day-ahead optimal scheduling

As already widely mentioned, the uncertainty in the performance of the day-ahead optimal scheduling is due to the variability of the input variables (direct and derived). In particular, this subsection aims to quantify, for the proposed case study, the impact of these uncertainty factors on the effectiveness of the control in term of: (i) prediction capacity of the models for SEHDs and for the indoor air temperature and (ii) variation in the control actions signals. The prediction capacity of the model is represented only by the RMSE evaluated on the indoor air temperature, since the temperatures of the storage materials in the SEHDs are not comparable with those measured. This is due to the fact that, variations in the direct and derived inputs can change the solution of the optimization problem (i.e., different control actions for the charging of the SEHDs).

As discussed in Section 6.2.1, the analysis can be reduced to the estimation of how the variability of direct inputs ($T_{outdoorF_k}$ and Cl_{F_k}) affects the results that can be obtained from the optimization problem. By isolating the contribution of each direct input, no significant changes are observed in the indoor air temperature trend predicted and in the charge control profile of the SEHDs when $T_{outdoorF_k}$ varies. Imposing as input Lig_{meas} and using the measure of the surplus PV generation to derive the weight w_1, the solution of the optimization problem by varying $T_{outddorF_k}$ does not allow to observe variation in the signals of charge of the devices and the RMSE of the internal air is always 0.44 °C. This may depend on two factors: the first is that the controlled room is not too much affected by the outdoor temperature because the room has only one (thermally insulated) wall facing outwards; the second is that $T_{outddorF_k}$ does not change significantly with the variation of k (Figs. 15a and 16a). In fact, the average daily outdoor temperature fluctuates between 13.9 °C and 14.2 °C with the variation of k, while its maximum variation varies between 7.7 °C and 9.7 °C.

On the other hand, a variation in performance is observed when the Cl prediction changes. In Fig. 20a, it can be observed that also in this case, as the average Cl changes, the prediction capacity of the model varies. In particular, with the increase of the average of Cl, the performance improves (RMSE passes from 0.52 °C to 0.31 °C, reduction of 40%). This can be seen more explicitly in Fig. 20b where the trends of $T_{a_{Fk}}$ in the two cases of extreme values of average Cl are reported: average Cl of 44% at k equal to 7 ($T_{a_{F7}}$) and 1% for k equal to 15 ($T_{a_{F15}}$).

As for the charge signals, these are highly dependent on the prediction of excess generation from PV and on how much the prediction of the internal air temperature deviates from the set-point. Both the weight function w_1 and the T_{aF_k} depend on the direct and derived input forecast and therefore, on the time k. If for the Heater 1, the same charging time is evaluated regardless of k, this does not happen for the second device (Heater 2). In Fig. 21 the number of hours in which the optimization problem assesses the need of charging the two SEHDs ($ctrl_{EH}$ equal to 1) is reported. Referring to the trend for the Heater 2 (blue curve in Fig. 21), the number of charging hours is 2 h in some cases, while in others it is 1 h. The difference between the solutions can be correlated to the variability of the inputs which, as we have seen, influence the expected internal air temperature and the prediction of PV surplus generation. In fact, it is noted that, as the maximum temperature reached by T_{aF_k} increases (green curve in Fig. 21), the number of hours in which $ctrl_{H2}$ is 1 decreases. However, this behaviour tends to be mitigated by the behaviour estimated for PV surplus. For k greater than 16, in which the

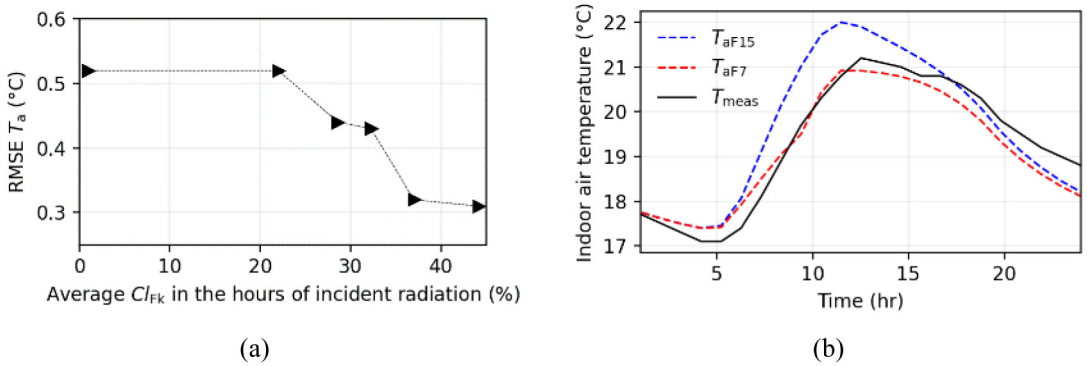

Fig. 20. Effect of input variability on the prediction capability of the model in the control: (a) RMSE of internal air temperature as function of average Cl in the hours of incident solar radiation and (b) comparison between the results of the model with two different input observation times (k = 7 and k = 15) and the measured indoor air temperature (2nd of May 2022).

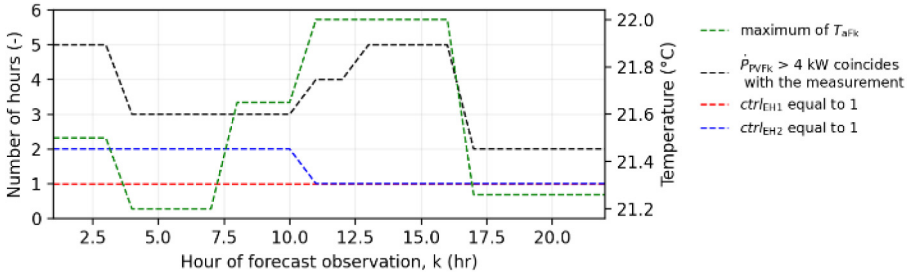

Fig. 21. Number of hours in which $ctrl_{EH1}$ and $ctrl_{EH2}$ are equals 1, maximum of the temperature predicted and number of hours in which the predicted PV surplus of more than 4 kW coincides with the measured as function of the time k in which the direct inputs are observed the day before (2nd of May 2022). (For interpretation of the references to colour in this figure legend, the reader is referred to the web version of this article.)

availability of PV is underestimated compared to the measurement (black line in Fig. 21), despite the maximum air temperature decreasing, there is no increase in charging hours of the heater. It can therefore be concluded that regarding Heater 2, due to the variability of inputs, the charging time of the device may vary from +100% to −50%. It is also worth specifying that the two SEHDs, as happens for k between 0 and 11, can have different control signals. However, with reference to this particular day, there is not any withdrawal of electricity from the grid. This is due to the effectiveness of the PV surplus generation model in correctly predicting the availability of electricity to charge the devices.

To conclude, the analysis showed how the uncertainty linked to some inputs has a considerable impact on the strategies decided by the control and on its prediction capability. In particular, Fig. 22 represents all the dependencies that have emerged, also highlighting the degree of uncertainty produced by the individual contributions.

As shown in Fig. 22, the most influential factors on the effectiveness of the predictive control are the presence of external disturbing factors and the unreliable prediction of some direct inputs (such as the cloudiness index). These uncertainties diminish the reliability of derived inputs (such as the total heat gains and the PV surplus).

Generalizing the results to wider applications (for example, larger multi-zones buildings) could result in even more noticeable performance variations, mainly due to the multiple disturbing factors and interference between the different contributions. Furthermore, in this work we implemented a day-ahead optimal scheduling. This aspect is very relevant because the uncertainty in inputs prediction decreases when the time horizon of the prediction is reduced. This could be improved with the implementation of a real-time optimal control with short prediction horizon (e.g., 1 h). However, it is also worth pointing out that, from the point of view of time effectiveness, the day-ahead optimal control is simpler and faster to implement. In fact, the computational time is very low, even if it can increase with the size of the problem considered. As future further development, a comparison between the performance of a day-ahead and a real time optimal control could be analysed to extend the considerations of this work.

Conclusions

The aim of this work is to provide a quantification of some of the main uncertainty factors in an optimal control really implemented in a building. A day-ahead optimal scheduling was applied to control the heating system of a single room in an office building. The heating system is composed of two smart electric heaters equipped with a thermal storage material. The controller is formulated to determine the charging periods of the storage materials in the heaters with the aim of minimizing the withdrawal of energy from the grid by being able to exploit a certain availability of energy from renewable sources and keeping the internal air temperature close to a setpoint imposed on the thermostat. The model contained in the optimal control is formulated to describe the thermal dynamics of the storage materials of the heaters and the indoor air temperature in the room. To be effective, the model requires some inputs on weather conditions and internal gains. These, in turn, are predicted through forecast models.

Firstly, the results of applying the control are shown: the effectiveness of the control is assessed independently of the assessment of the uncertainties on the predicted inputs. The control demonstrated good performance in terms of predicting the thermal dynamic of the system. Considering the two days in which

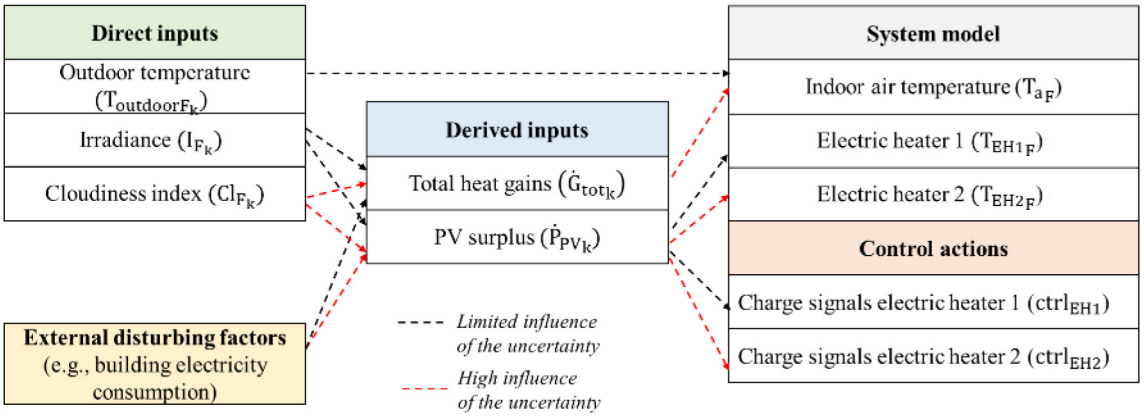

Fig. 22. Graphical representation of the impact of the individual factors of uncertainty.

the controller was actually applied, RMSEs of 0.36 °C and 0.52 °C were obtained by comparing the indoor air temperature prediction with that actually measured by applying the control. Good performances were also obtained for the thermal dynamics of the storage materials: relative error of the temperature of the storage materials in the electric heaters lower than 13.2%. On the other hand, the performance of the control was not so good when considering the exploitation of energy from the renewable source (i.e., PV panels), especially on the second test day (May 4, 2022). This is attributable to the inaccuracy of the models for the prediction of the inputs, including that for surplus PV generation. Analysing this last aspect, in the second part of the discussion, it was evaluated how the inaccuracy on direct and derived inputs affects the performance of the control causing uncertainties. In this regard, the main conclusions that emerged can be summarized as follows:

- In general, the effectiveness of the control is very dependent on forecasting models of weather conditions. These were obtained from traditional numerical prediction models downloadable from an online database (identified in the text of the paper with the term direct inputs). This creates underlying control uncertainty.
  This is an issue that cannot be overlooked when it comes to applying optimal control in the absence of measured on-site weather data.
- The estimate of the total heat gains (inputs derived from models developed by the authors) proved to be very affected by the uncertainty related to weather conditions (especially the cloudiness index which has shown to be very dependent on the moment in which the forecasts are observed)
- The prediction of the availability of surplus PV generation (second input derived from the forecast model) shown to be significantly dependent on the uncertainty linked to the observation of the cloudiness index (percentage of time in which the prediction is similar to the measurements varies between 21% and 47%).
- The uncertainty of the prediction of direct and derived inputs influences the control actions. In relation to the characteristics of the case study analysed (i.e., building with only one external wall with a large-windowed surface), the prediction capacity of the system model did not show evident dependencies on the uncertainty related to the forecast of the external temperature. On the other hand, once again, the cloudiness index has the greatest influence on the accuracy of the control. This greatly affects the control actions defined by the controller. It has been observed that for one of the two electric heaters, the estimated charging time can vary from −50% to +100% depending on when the forecast is observed. This has an effect, albeit limited, also on the prediction of the internal air temperature: considering the extreme values, a 40% change in RMSE (calculated comparing predicted and measured indoor air temperature) was assessed.

It is important to underline that these considerations are obviously related to the characteristics of the case study and to the architecture of the models used. It is also not possible to exclude a non-negligible effect of some disturbing factors not included in the modelling (e.g., opening windows or consumption behaviour of the occupants). As a future development it would be interesting to extend the uncertainty analysis considering different model architectures. In general, however, we can conclude that our analysis showed a non-negligible influence of the uncertainties due to the prediction of the inputs on the actual performance of the control. This confirms the need for further studies on the effective application of advanced control techniques in buildings and on methods to decrease the impact of such uncertainty in a way easy to be implemented in practice.

Nomenclature

a	Parameter obtained from the training
b	Parameter obtained from the training
c	Parameter obtained from the training
C	Thermal capacity (Wh K^{-1})
Cl	Cloudiness index (%)
ctrl	Charge signal
EH	Electric heater
F	Scale factor
f	Parameter obtained from the training
$\dot{G}$	Total heat gains (W)
GDH	Glen Dimplex Heaters
h	Hour of the day
I	Irradiance (W m^{-2})
IEA	International Energy Agency
IoT	Internet of Things
K	Conductances (W K^{-1})
l	Parameter obtained from the training
Lig	Illuminance (lx)
MPC	Model Predictive Control
p	parameter obtained from the training
$\dot{P}$	Electric power (W)
pdf	Probability density function
PV	Photovoltaic plant

$\dot{Q}$	Thermal power (W)
RBC	Rule Based-Controller
RC	Resistance and Capacity network
RES	Renewable Energy Source
RMPC	Robust Model Predictive Controls
RMSE	Root Mean Square Error
$\dot{S}$	Gain (W)
SBC	Schedule-Based Controller
SEHD	Smart Electric Heating Devices
SMPC	Stochastic Model Predictive Controls
T	Temperature (°C)
t	Time (h)
TES	Thermal Energy Storage
v	Speed (m s^{-2})
w	Weights assigned to the individual objective in the optimization problem
ΔT	Tolerance in temperature (°C)

Subscripts

outdoor	Outdoor
F	Forecast
a	Indoor air
e	Relating to the power exchanged at the general meter
EH	Electric Heater
FAN	Relating to the fan of the electric heater
g	Relating to total heat gains
int	Relating to internal gains
k	Time in which the forecast is observed
l	Relating to thermal losses
max	Relating to the maximum value
meas	Measured
min	Relating to the minimum value
PV	Relating to photovoltaic
sol	Relating to solar gains
sp	Relating to the setpoint
T	Threshold
th	Relating to the thermostat
tot	Total
wa	Relating to the mass of the building envelope towards the internal air
wind	Relating to the thermal insulation layer
wins	Relating to the windows
wo	Relating to the mass of the building envelope towards the external

CRediT authorship contribution statement

A. Mugnini: Conceptualization, Methodology, Software, Validation, Writing – original draft, Formal analysis. **F. Ferracuti:** Conceptualization, Methodology, Software, Validation, Writing – review & editing. **M. Lorenzetti:** Visualization, Supervision. **G. Comodi:** Methodology, Supervision, Project administration, Funding acquisition. **A. Arteconi:** Conceptualization, Methodology, Writing – review & editing, Visualization, Supervision.

Declaration of competing interest

The authors declare that they have no known competing financial interests or personal relationships that could have appeared to influence the work reported in this paper.

Data availability

The data that has been used is confidential.

Acknowledgement

This study has received funding from European Union's Horizon 2020 Research and Innovation programme under grant agreement No 824441 (MUSE GRIDS).

References

Barber, Kyle A., Krarti, Moncef, 2022. A review of optimization based tools for design and control of building energy systems. Renew. Sustain. Energy Rev. 160, 112359. http://dx.doi.org/10.1016/j.rser.2022.112359.

Beal, L.D.R., Hill, D., Martin, R.A., Hedengren, J.D., 2018. GEKKO optimization suite. Processes 6 (8), http://dx.doi.org/10.3390/pr6080106.

Boodi, A., Beddiar, K., Amirat, Y., Benbouzid, M., 2020. Simplified building thermal model development and parameters evaluation using a stochastic approach. Energies 13 (11), 2899. http://dx.doi.org/10.3390/en13112899.

Ceusters, Glenn, Rodríguez, Román Cantú, García, Alberte Bouso, Franke, Rüdiger, Deconinck, Geert, Helsen, Lieve, Nowé, Ann, Messagie, Maarten, Camargo, Luis Ramirez, 2021. Model-predictive control and reinforcement learning in multi-energy system case studies. Appl. Energy 303, 117634. http://dx.doi.org/10.1016/j.apenergy.2021.11763.

Dounis, A.I., Caraiscos, C., 2009. Advanced control systems engineering for energy and comfort management in a building environment—A review. Renew. Sustain. Energy Rev. 13 (6–7), 1246–1261. http://dx.doi.org/10.1016/j.rser.2008.09.01.

Drgoňa, Ján, Arroyo, Javier, Figueroa, Iago Cupeiro, Blum, David, Arendt, Krzysztof, Kim, Donghun, Ollé, Enric Perarnau, Oravec, Juraj, Wetter, Michael, Vrabie, Draguna L., Helsen, Lieve, 2020. All you need to know about model predictive control for buildings. Annu. Rev. Control 50, 190–232. http://dx.doi.org/10.1016/j.arcontrol.2020.09.001.

Eurostat, 2022. European Union, Energy consumption in households. https://ec.europa.eu/eurostat/statistics-explained/index.php?title=Energy_consumption_in_households (access verified on 2/08/2022).

Glen dimplex, 2022. Thecnical specifications electric heater (Quantum Heater QM). Catalog available at www.dimplex.co.uk/sites/default/files/assets//Dimplex%20Quantum%20Spec%20Sheet%20Issue%207.pdf (access verified on 25/08/2022).

Hoseinpoori, Pooya, Olympios, Andreas V., Markides, Christos N., Woods, Jeremy, Shah, Nilay, 2022. A whole-system approach for quantifying the value of smart electrification for decarbonising heating in buildings. Energy Convers. Manage. 268, 115952. http://dx.doi.org/10.1016/j.enconman.2022.115952.

Hou, Juan, Li, Haoran, Nord, Natasa, Huang, Gongsheng, 2022. Model predictive control under weather forecast uncertainty for HVAC systems in university buildings. Energy Build. 257, 111793. http://dx.doi.org/10.1016/j.enbuild.2021.111793.

International Energy Agency (IEA), 2022a. Buildings. A source of enormous untapped efficiency potential. https://prod.iea.org/topics/buildings (access verified on 2/08/2022).

International Energy Agency (IEA), 2022b. Heat Pumps. https://www.iea.org/reports/heat-pumps (access verified on 2/08/2022).

International Energy Agency (IEA), 2022c. Tracking Buildings 2021. https://www.iea.org/reports/tracking-buildings-2021 (access verified on 2/08/2022).

Jensen, Søren Østergaard, Marszal-Pomianowska, Anna, Lollini, Roberto, Pasut, Wilmer, Knotzer, Armin, Engelmann, Peter, Stafford, Anne, Reynders, Glenn, 2017. IEA EBC annex 67 energy flexible buildings. Energy Build. 155, 25–34. http://dx.doi.org/10.1016/j.enbuild.2017.08.044.

Kontes, Georgios D., Giannakis, Georgios I., Sánchez, Víctor, Agustin-Camacho, Pablo De, Romero-Amorrortu, Ander, Panagiotidou, Natalia, Rovas, Dimitrios V., Steiger, Simone, Mutschler, Christopher, Gruen, Gunnar, 2018. Simulation-based evaluation and optimization of control strategies in buildings. Energies 11 (12), 3376. http://dx.doi.org/10.3390/en11123376.

Krarti, Moncef, 2018. Chapter 3 - Control strategies for building energy systems. In: Krarti, Moncef (Ed.), Optimal Design and Retrofit of Energy Efficient Buildings, Communities, and Urban Centers. Butterworth-Heinemann, pp. 117–187. http://dx.doi.org/10.1016/B978-0-12-849869-9.00003-X.

Li, Yanfei, O'Neill, Zheng, Zhang, Liang, Chen, Jianli, Im, Piljae, DeGraw, Jason, 2021. Grey-box modeling and application for building energy simulations - A critical review. Renew. Sustain. Energy Rev. 146, 111174. http://dx.doi.org/10.1016/j.rser.2021.111174.

Lin, Jing, Fernández, Julián A., Rayhana, Rakiba, Zaji, Amirhossein, Zhang, Ran, Herrera, Omar E., Liu, Zheng, Mérida, Walter, 2022. Predictive analytics

for building power demand: Day-ahead forecasting and anomaly prediction. Energy Build. 255, 111670. http://dx.doi.org/10.1016/j.enbuild.2021.111670.

Lu, Yuehong, Wang, Shengwei, Sun, Yongjun, Yan, Chengchu, 2015. Optimal scheduling of buildings with energy generation and thermal energy storage under dynamic electricity pricing using mixed-integer nonlinear programming. Appl. Energy 147, 49–58. http://dx.doi.org/10.1016/j.apenergy.2015.02.060.

Lyons, Ben, O'Dwyer, Edward, Shah, Nilay, 2020. Model reduction for Model Predictive Control of district and communal heating systems within co-operative energy systems. Energy (ISSN: 0360-5442) 197, 117178. http://dx.doi.org/10.1016/j.energy.2020.117178.

Ma, Y., Matuško, J., Borrelli, F., 2015. Stochastic model predictive control for building HVAC systems: Complexity and conservatism. IEEE Trans. Control Syst. Technol. 23 (1), 101–116. http://dx.doi.org/10.1109/TCST.2014.2313736.

Maasoumy, M., Razmara, M., Shahbakhti, M., Sangiovanni Vincentelli, A., 2014. Handling model uncertainty in model predictive control for energy efficient buildings. Energy Build. 77, 377–392. http://dx.doi.org/10.1016/j.enbuild.2014.03.057.

Marvuglia, Antonino, Messineo, Antonio, Nicolosi, Giuseppina, 2014. Coupling a neural network temperature predictor and a fuzzy logic controller to perform thermal comfort regulation in an office building. Build. Environ. 72, 287–299. http://dx.doi.org/10.1016/j.buildenv.2013.10.020.

Mayne, D.Q., Rawlings, J.B., Rao, C.V., Scokaert, P.O.M., 2000. Constrained model predictive control: Stability and optimality. Automatica 36 (6), 789–814. http://dx.doi.org/10.1016/S0005-1098(99)00214-9.

Mugnini, Alice, Coccia, Gianluca, Polonara, Fabio, Arteconi, Alessia, 2020. Performance assessment of data-driven and physical-based models to predict building energy demand in model predictive controls. Energies 13 (12), 3125. http://dx.doi.org/10.3390/en13123125.

Mugnini, A., Coccia, G., Polonara, F., Arteconi, A., 2021. Energy flexibility as additional energy source in multi-energy systems with district cooling. Energies 14 (2), 519. http://dx.doi.org/10.3390/en14020519.

Mugnini, A., Ferracuti, F., Lorenzetti, M., Comodi, G., Arteconi, A., 2022. Advanced control techniques for CHP-DH systems: A critical comparison of model predictive control and reinforcement learning. Energy Convers. Manage. X 15, 100264. http://dx.doi.org/10.1016/j.ecmx.2022.100264.

Oldewurtel, F., Parisio, A., Jones, C., Morari, M., Gyalistras, D., Gwerder, M., Stauch, V., Lehmann, B., Wirth, K., 2010. Energy efficient building climate control using stochastic model predictive control and weather predictions. In: Proc. of American Control Conference.

Péan, Thibault Q., Salom, Jaume, Costa-Castelló, Ramon, 2019. Review of control strategies for improving the energy flexibility provided by heat pump systems in buildings. J. Process Control 74, 35–49. http://dx.doi.org/10.1016/j.jprocont.2018.03.006.

Petersen, Steffen, Bundgaard, Katrine Wieck, 2014. The effect of weather forecast uncertainty on a predictive control concept for building systems operation. Appl. Energy (ISSN: 0306-2619) 116, 311–321. http://dx.doi.org/10.1016/j.apenergy.2013.11.060.

Ramos, José Sánchez, Moreno, Mcarmen Pavón, Delgado, Mcarmen Guerrero, Domínguez, Servando Álvarez, Cabeza, Luisa F., 2019. Potential of energy flexible buildings: Evaluation of DSM strategies using building thermal mass. Energy Build. 203, 109442. http://dx.doi.org/10.1016/j.enbuild.2019.109442.

Sampaio, Phillipe R., Salvazet, Raphael, Mandel, Pierre, Becker, Gwénaëlle, Chenu, Damien, 2021. Simulation and optimal control of heating and cooling systems: A case study of a commercial building. Energy Build. (ISSN: 0378-7788) 246, 111102. http://dx.doi.org/10.1016/j.enbuild.2021.111102.

Serale, G., Fiorentini, M., Capozzoli, A., Bernardini, D., Bemporad, A., 2018. Model predictive control (MPC) for enhancing building and HVAC system energy efficiency: Problem formulation, applications and opportunities. Energies 11, 631.

Sharma, Himanshu, Bhattacharya, Saptarshi, Kundu, Soumya, Adetola, Veronica A., 2022. On the impacts of occupancy sensing on advanced model predictive controls in commercial buildings. Build. Environ. 109372. http://dx.doi.org/10.1016/j.buildenv.2022.109372.

Stinner, Sebastian, Huchtemann, Kristian, Müller, Dirk, 2016. Quantifying the operational flexibility of building energy systems with thermal energy storages. Appl. Energy 181, 140–154. http://dx.doi.org/10.1016/j.apenergy.2016.08.055.

Tien, Paig Wenbin, Wei, Shuangyu, Darkwa, Jo, Wood, Christopher, Calautit, John Kaiser, 2022. Machine learning and deep learning methods for enhancing building energy efficiency and indoor environmental quality – A review. Energy AI 10, 100198. http://dx.doi.org/10.1016/j.egyai.2022.100198.

UNI (Italian Standard Organization), 2014. Energy Performance of Buildings - Part 1: Evaluation of Energy Need for Space Heating and Cooling (Italian Standard). UNI/TS 11300-1, Date of entry into force: 02 October 2014.

UNI (Italian Standard Organization), 2018a. Building Components and Building Elements - Thermal Resistance and Thermal Transmittance - Calculation Methods (Italian Standard). UNI EN ISO 6946, Date of entry into force: 01 March 2018.

UNI (Italian Standard Organization), 2018b. Thermal Performance of Buildings - Heat Transfer Via the Ground - Calculation Methods (Italian Standard). UNI EN ISO 13370, Date of entry into force: 01 March 2018.

UNI (Italian Standard Organization), 2018c. Energy Performance of Buildings - Method for Calculation of the Design Heat Load. UNI EN 12831, Date of entry into force: 22 February 2018.

UNI (Italian Standard Organization), 2018d. Thermal Performance of Windows, Doors and Shutters - Calculation of Thermal Transmittance. UNI EN ISO 10077, Date of entry into force: 01 March 2018.

Vakiloroaya, Vahid, Samali, Bijan, Fakhar, Ahmad, Pishghadam, Kambiz, 2014. A review of different strategies for HVAC energy saving. Energy Convers. Manage. 77, 738–754. http://dx.doi.org/10.1016/j.enconman.2013.10.023.